Journal of Power Sources 243 (2013) 299–305

Contents lists available at SciVerse ScienceDirect

Journal of Power Sources

journal homepage: www.elsevier.com/locate/jpowsour

Ru-capped/FeCo nanoflowers with high catalytic efficiency towards hydrolytic dehydrogenation

Ming Wen [a,b,*], Yuzhen Sun [a], Xiaomeng Li [a], Qingsheng Wu [a,b], Qingnan Wu [a], Chenxiang Wang [a]

[a] Department of Chemistry, Key Laboratory of Yangtze River Water Environment, Ministry of Education, Tongji University, Shanghai, China
[b] Shanghai Key Lab Development & Applicat Metal Function Material, Tongji University, Shanghai, China

HIGHLIGHTS

- Newly designed Ru-capped/FeCo nanoflowers are reported in this work.
- Ru-capped/FeCo nanoflowers exhibit high catalytic dehydrogenation of $NaBH_4$.
- The Ru-capped/FeCo nanoflowers can be recovered and recycled.
- Ru-capped/FeCo nanoflowers have potential applications in hydrogen energy.

GRAPHICAL ABSTRACT

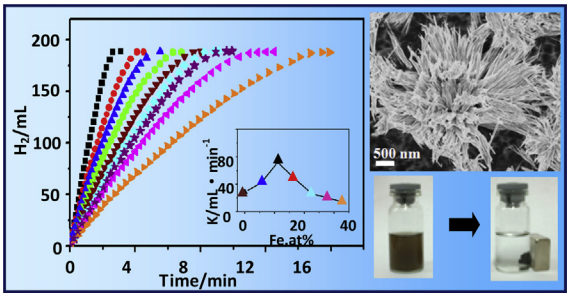

ARTICLE INFO

Article history:
Received 29 May 2013
Accepted 30 May 2013
Available online 12 June 2013

Keywords:
Nanoflowers
Catalysis
Dehydrogenation
Sodium borohydride

ABSTRACT

Magnetic Ru-capped/FeCo nanoflowers are solvothermally synthesised through a self-catalytic growth and assembly process. The synthesised Ru-capped/FeCo nanoflowers (~3.63 μm) consist of Ru-capped FeCo nanorods with an average diameter of ~13 nm and a length ranging from 1.33 to 2.1 μm. A vibration sample magnetometer measurement reveals that the ferromagnetic behaviours depend on nanomaterial composition. Particularly, an appropriate quantity of Fe in the composition improved catalytic activity. The $Fe_{22}Co_{73}/Ru_5$ nanoflowers exhibits the highest catalytic activity towards $NaBH_4$ hydrolytic dehydrogenation at ambient pressure and room temperature (the dehydrogenation rate is 4293.75 mL min^{-1} g^{-1}; the activation energy is 42.95 kJ mol^{-1}).

1. Introduction

Multimetallics hold promise for new nanomaterials with desired catalytic, magnetic and optical properties. The superior performance of multimetallic nanomaterials distinguishes them from their monometallic counterparts [1]. Particularly, hierarchically structured three-dimensional (3D) multimetallic nanomaterials can be specifically tailored to exploit the synergistic effects between the individual metals [2–11]. Significant economic incentives exist for fabricating 3D hierarchical nanostructures with noble metal surfaces because of the noble elements' high surface areas relative to their atomic volumes. In addition, incorporating magnetic building blocks (Fe, Co and Ni) facilitates nanomaterial recyclability [12–20]. However, obstacles remain for synthesising multimetallic hierarchical nanostructures because of several physicochemical factors (e.g., cohesive energy, surface energy) [10,21].

* Corresponding author. Department of Chemistry, Tongji University, Shanghai, China. Tel.: +86 21 65982653x8544; fax: +86 21 65981097.
E-mail address: m_wen@tongji.edu.cn (M. Wen).

0378-7753
http://dx.doi.org/10.1016/j.jpowsour.2013.05.190

Although ruthenium (Ru) is the active catalytic component for many reactions, investigation of Ru-containing multimetallic nanomaterials has thus far been limited mostly to the FeCo/Ru system [9,22–26]. The development of Ru-containing hierarchical nanostructures with optimised properties, therefore, is both interesting and promising. Because catalytic reactions occur mainly at the surfaces of nanoparticles (NPs), magnetic FeCo nanoflowers capped with Ru were desired to optimise Ru catalytic activity.

Compared with the numerous sources of hydrogen, $NaBH_4$ possesses a high hydrogen capacity (10.8 wt%), is non-flammable, non-toxic, [27] and has a most commonly produced hydrolysis product ($NaBO_2$) that is harmless and can be regenerated to $NaBH_4$ [28,29]. Hence, $NaBH_4$ is widely appraised as a competitive candidate for an effective hydrogen storage medium. Generally, $NaBH_4$ hydrolysis is confined to pH above 13; therefore, under ambient pressure, catalysts are required for efficient hydrogen release. To be practical, these catalysts must be efficient, economical and recyclable under moderate conditions [30–36].

In this work, magnetic Ru-capped/FeCo nanoflowers are solvothermally synthesised by a self-catalytic growth and assembly process. The catalytic activity of the synthesised nanoflowers towards $NaBH_4$ hydrolytic dehydrogenation at ambient pressure is investigated thoroughly. It is indicated that the synergistic effect of FeCo and Ru in the hierarchically structured cap-nanoflowers contributes to their excellent catalytic activity.

2. Experimental

2.1. Chemicals

Ruthenium chloride ($RuCl_3 \cdot nH_2O$, 98%) was purchased from Aldrich. Iron oxalate ($Fe_2(C_2O_4)_3 \cdot 5H_2O$, 95%), anhydrous cobalt acetate ($Co(CH_3COO)_2 \cdot 4H_2O$, 99%), sodium borohydride ($NaBH_4$, 99%), sodium hydroxide (NaOH, 99%), ethanol (C_2H_5OH, 99%), and ethylene glycol ($C_2H_6O_2$, 99%) were purchased from Sinopharm Chemical Reagent Co., Ltd (SCRC). All reagents were used without further purification.

2.2. Synthesis of FeCo/Ru cap-nanoflowers

3D Ru-capped/FeCo nanoflowers were fabricated by a solvothermal synthesis. $RuCl_3 \cdot nH_2O$, $Fe_2(C_2O_4)_3 \cdot 5H_2O$ and $Co(CH_3COO)_2 \cdot 4H_2O$ were used as precursors. The synthesis of $Fe_{45}Co_{50}/Ru_5$ cap-nanoflowers typifies the procedure: 2 mL ethyl alcohol was mixed with 0.3 mM Fe^{3+}, 0.3 mM Co^{2+} and 0.031 mM Ru^{3+} at room temperature. 7 mL of ethylene glycol was added, and then the mixture was placed in an autoclave. After sealing, the reaction system was heated at a rate of 1 °C min^{-1} from room temperature (r.t.) to 180 °C and held at 180 °C for 15 h. The reaction was cooled to room temperature, and the resultant $Fe_{45}Co_{50}/Ru_5$ was collected from the bottom of the container. The product was washed with ethanol, centrifuged, washed with deionised water, and then centrifuged. This washing sequence was repeated two more times. Finally, the products were vacuum dried. The remaining FeCo/Ru nanoalloys were prepared using the following initial Fe^{3+}:Co^{2+}:Ru^{3+} molar ratios: 67:28:5, 57:38:5, 47.5:47.5:5, 34:61:5, 24:71:5, and 15:80:5 for $Fe_{65}Co_{30}/Ru_5$, $Fe_{55}Co_{40}/Ru_5$, $Fe_{45}Co_{50}/Ru_5$, $Fe_{32}Co_{63}/Ru_5$, $Fe_{22}Co_{73}/Ru_5$ and $Fe_{11}Co_{84}/Ru_5$, respectively.

2.3. Test for catalytic activity in dehydrogenation

To evaluate the catalytic properties of the synthesised products, we measured their catalytic activities towards $NaBH_4$ dehydrogenation. Typically, $NaBH_4$ (0.21 M), NaOH (0.375 M), and 10 mL deionised water were added to a one-necked round-bottom flask. The catalysts (16.0 mg FeCo/Ru nanoalloys) were then added into the reaction solution in a single charge. The reaction was allowed to progress at room temperature under constant electric stirring. The volume of hydrogen gas generated from the hydrolysis reaction was measured using the water-replaced method. In all of the experiments, the generated hydrogen was passed through 98% H_2SO_4 to remove water vapour.

2.4. Characterisation

Field-emission scanning electron microscopy (FE-SEM, JEOL, S-4800, Hitachi, Japan) was used to investigate the size and morphology of the samples. Microstructural properties were studied by transmission electron microscopy (TEM) and high resolution TEM (HRTEM). Both types of TEM images were obtained using a JEOL JEM-1200EX microscope (Japan). Elemental analysis was conducted by inductively coupled plasma atomic emission spectroscopy (ICP-AES) on an ICAP6300 instrument (Thermo Fisher Scientific, USA); the results were confirmed on selected sample areas by energy-dispersive X-ray spectroscopy (EDS), which was conducted at 20 keV on a TN5400 EDS instrument (Oxford). Powder X-ray diffraction (XRD) patterns were obtained using a Bruker D8 (German) diffractometer with a Cu Kα radiation source ($\lambda = 0.154056$ nm). X-ray photoelectron spectroscopy (XPS) experiments were performed on an RBD-upgraded PHI–5000C ESCA system (Perkin Elmer) using Al Kα radiation ($h\nu = 1486.6$ eV). The whole XPS spectrum (0–1100 eV) and the narrower, high-resolution spectra were all recorded using an RBD 147 interface (RBD Enterprises, USA) and AugerScan 3.21 software. Binding energies were calibrated using the containment carbon (C1s = 284.6 eV). A lakeshore-735 vibration sample magnetometer (VSM, USA) instrument was used to examine the magnetic properties of synthesised products. Detailed magnetic data of the samples with respect to their individual Fe:Co:Ru alloy content are summarized in Table 1.

3. Results and discussion

3.1. Synthetic mechanism

The solvothermal synthesis of Ru-capped/FeCo nanoflowers proceeded by the reductive and alloying process of Ru^{3+}, Fe^{3+}, and Co^{2+} by ethylene glycol, as shown in Scheme 1. In the first reaction stage, Ru^{3+} was reduced to Ru^0. When the Ru concentration reached the point of supersaturation [36], Ru atoms aggregated into nuclei. The Ru nuclei then rapidly grew into Ru nanocrystals of ~3 nm—an average size dictated by the amount of Ru^{3+} available in our studied reaction system. In the second reaction stage, the surface of these Ru nanocrystal caps catalysed the reduction of Fe^{3+} and Co^{2+} to the FeCo alloy. Because no surface, catalytic system creates anisotropic growth dependent upon an underlying FeCo crystal structure, growth occurred preferentially along the FeCo/Ru cap axis during the slow, ~1 °C min^{-1} heating from r.t. to 180 °C, and this growth was autocatalytic. The subsequent 15 h heat

Table 1
Initial molar ratios of Fe^{3+}:Co^{2+}:Ru^{3+} and compositions of synthesised FeCo/Ru nanoalloys with corresponding magnetisation (*Ms*) and coercivity (*Hc*).

Sample No.	Initial molar ratios of Fe^{3+}:Co^{2+}:Ru^{3+}	Alloy content (at.%)	*Hc* (Oe)	*Ms* (emu g^{-1})
S-a	67:28:5	$Fe_{65}Co_{30}/Ru_5$	213.31	173.39
S-b	57:38:5	$Fe_{55}Co_{40}/Ru_5$	264.16	155.01
S-c	47.5:47.5:5	$Fe_{45}Co_{50}/Ru_5$	309.96	136.88
S-d	34:61:5	$Fe_{32}Co_{63}/Ru_5$	378.16	118.81
S-e	24:71:5	$Fe_{22}Co_{73}/Ru_5$	708.14	105.61
S-f	15:80:5	$Fe_{11}Co_{84}/Ru_5$	534.11	90.12

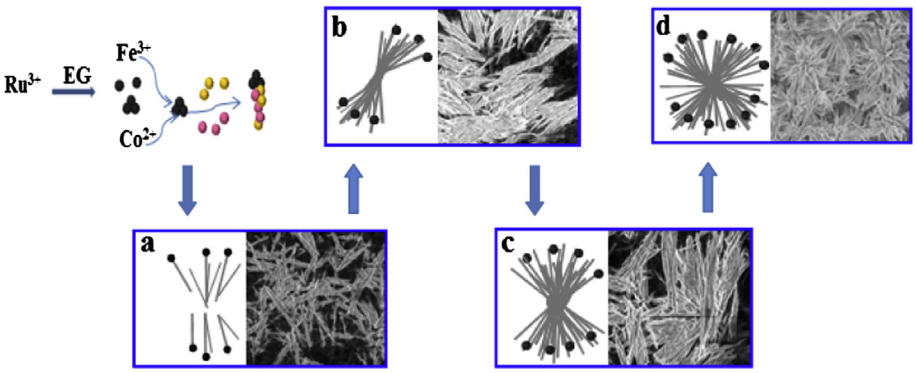

Scheme 1. Schematic view of the assembly process of Ru-capped/FeCo nanoflowers with inset SEM images obtained at heating times 1 (a), 5 (b), 10 (c) and 15 h (d), respectively.

treatment further promoted the self-assembly of FeCo/Ru cap-nanoflowers. SEM images obtained at different reaction times (Scheme 1a–d) clearly showed that FeCo/Ru nanorod assembly led to hierarchical nanostructure formation: from FeCo/Ru cap-nanobrooms to cap-nanoflowers.

3.2. Morphologies and structures

Product morphologies are characterised by SEM and TEM and are shown in Fig. 1. The synthesised Ru-capped/FeCo nanoflowers assembled from FeCo/Ru nanorods has an average diameter of ~3.63 μm (Fig. 1A), and the Ru-caps are observed on the surface of nanoflowers. In Fig. 1B and C, TEM images contrast the grey FeCo nanorods (Nds) and with their dark Ru nano-caps. In these two figures, the FeCo nanorods have an average diameter of ~13 nm, whereas the Ru nano-caps are ~ 15 nm and comprised NPs of ~3 nm. EDS performed on the dark metallic caps (Spectrum (A)) and grey rods (Spectrum (B)) unambiguously identified the caps as Ru and the rods as alloys of Fe and Co in an ~1/1 ratio (Fig. 1D). In the inset of Fig. 2B, the SAED pattern recorded from FeCo Nds exhibits a diffuse halo that indicated an amorphous structure. This observation is consistent with the XRD pattern, whose broad halo implied a chemically disordered and amorphous structure ((c) in Fig. 2F). The HRTEM image (Fig. 1C upper inset) of Ru nano-caps illustrates its crystalline structure with an average lattice spacing of ~0.246 nm corresponding to Ru (101) plane spacing. The selected-area electron diffraction (SAED) pattern of Ru NPs (Fig. 1C lower inset) exhibits the crystalline spots ring indicative of a polycrystalline structure.

Because the initial stoichiometric composition plays an important role in the final FeCo/Ru nanostructure, we have thoroughly compared the morphologies of a series of FeCo/Ru nanoalloys made from differing amounts of Fe and Co starting material (at. %). Fig. 2

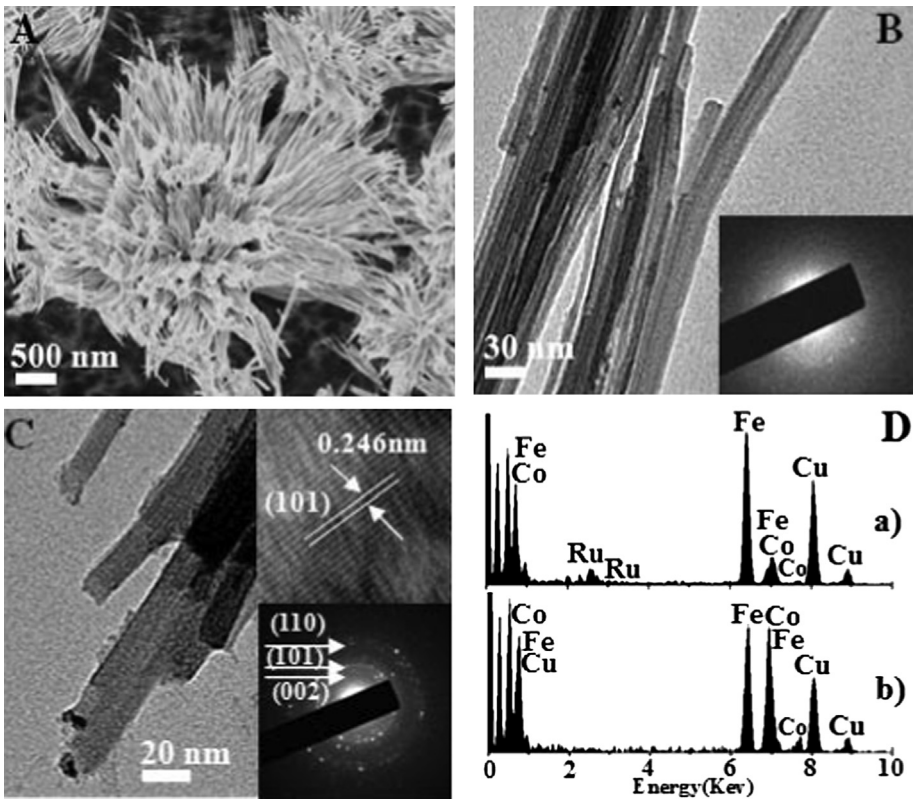

Fig. 1. A) SEM image of FeCo/Ru cap-nanoflowers; B) TEM image of FeCo nanorods with inset SADP; C) TEM image of FeCo/Ru cap-nanorods with upper inset HRTEM image and lower inset SADP of Ru nanocap; D) selected area EDXS of FeCo/Ru (a) and FeCo nanorods (b).

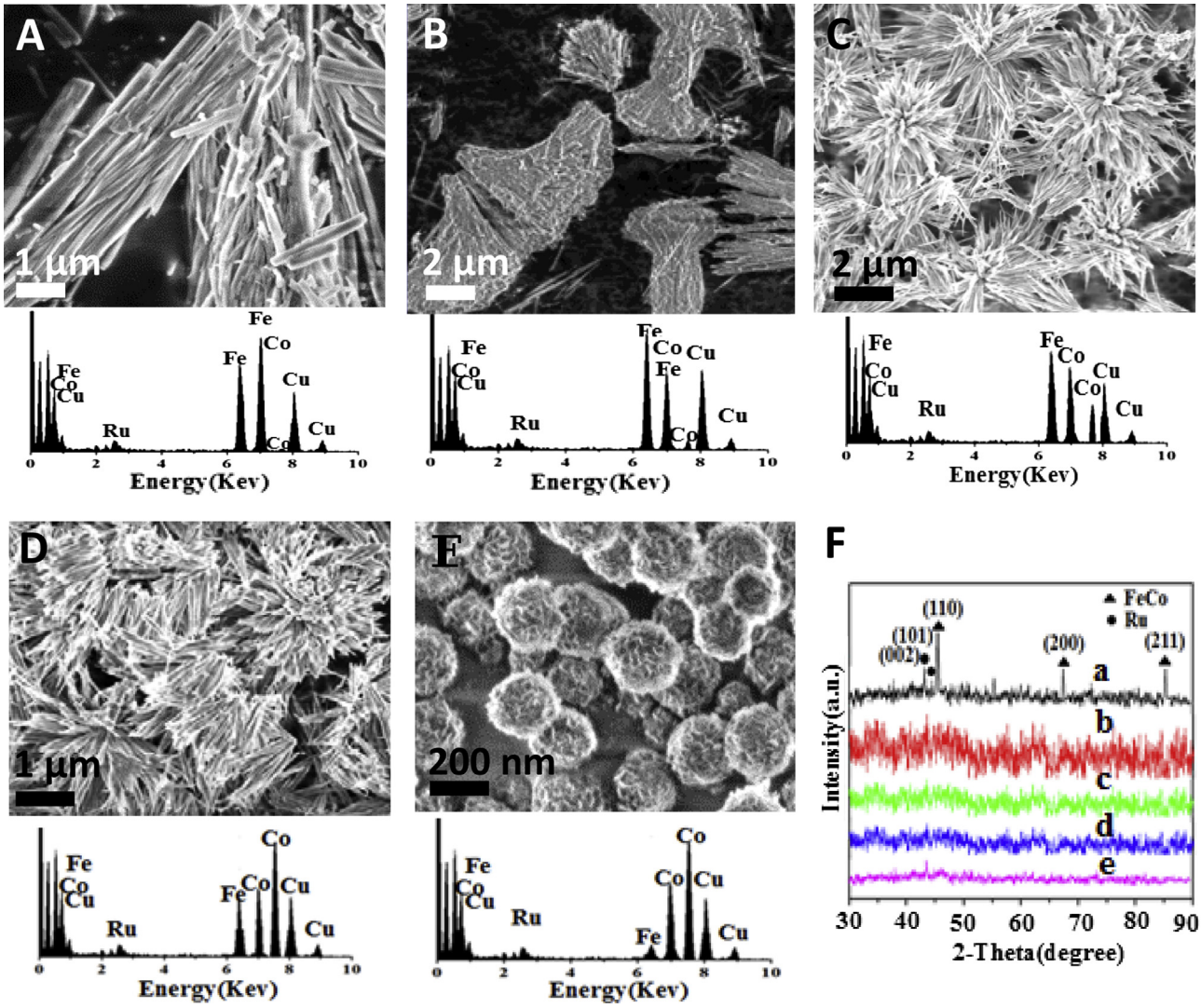

Fig. 2. (A–E) SEM images with corresponding EDS spectra of FeCo/Ru nanostructures in differing compositions: $Fe_{65}Co_{30}/Ru_5$, $Fe_{55}Co_{40}/Ru_5$, $Fe_{45}Co_{50}/Ru_5$, $Fe_{22}Co_{73}/Ru_5$, and $Fe_{11}Co_{84}/Ru_5$, respectively; (F) corresponding XRD patterns for the samples (b–e) and the annealed sample (a).

comprises SEM images and corresponding EDS spectra, of FeCo/Ru nanoalloys in different Fe:Co molar ratios. The compositions were confirmed by ICP-AES elemental analysis, and those ICP results are listed in Table 1. As the Fe content decreased, the shapes changed sequentially from bundled-nanorods to nanoflowers to nanospheres. Fe-rich $Fe_{65}Co_{30}/Ru_5$ and $Fe_{55}Co_{40}/Ru_5$ were bundled-nanorods, whereas $Fe_{45}Co_{50}/Ru_5$ and $Fe_{22}Co_{73}/Ru_5$ were cap-nanoflowers. Only $Fe_{11}Co_{84}/Ru_5$ gave rise to nanospheres. The lengths of the FeCo nanorods, which were considerable, increased with higher Fe content. The Ru-capped/FeCo nanoflowers consisted of Ru-capped FeCo nanorods ranging in length from 1.33 to 2.1 μm. As shown in Fig. 2F, the XRD patterns of all synthesised FeCo/Ru nanostructures had two broad halos, (110) at ~45° and (200) at ~65.5°, corresponding to standard face-centred cubic (fcc) structures with random crystalline orientations [33]. These XRD data are consistent with the chemically disordered and amorphous structure suggested by the diffuse halo in the SADP inset of Fig. 1B. After being annealed at 773 K under argon, the FeCo/Ru nanoalloys transformed into long-range, chemically ordered fcc structures, as shown by the XRD pattern (a) in Fig. 2F. This XRD pattern is consistent with the bulk FeCo crystal structure and the RU face-centred cubic structure.

The hierarchically structured Ru-capped/FeCo nanoflowers were also analysed by XPS. Fig. 3A shows the five XPS photoemission peaks of Fe45Co50/Ru5 cap-nanoflowers corresponding to Fe *2p*, Co *2p*, C *1s*, O *1s*, Ru *3d* and Ru *3p*. The Fe *2p* peaks (710.8 and 720.1 eV) are magnified because of the spin-orbit splitting of $2p_{3/2}$ and $2p_{1/2}$ (Fig. 3B), indicating that Fe (III) and Fe (0) are dominant on the surface of the product. In Fig. 3C, the Co multiplet resulted from *2p* splitting into $2p_{3/2}$ and $2p_{1/2}$ with binding energy (BE) values of 778.2 and 793.5 eV, respectively, indicative of Co (0). The 279.4 eV $3d_{5/2}$ and 283.5 eV $3d_{3/2}$ peaks of Ru (0) from the spin-orbit splitting of Ru *3d* are shown in Fig. 3D. Additionally, two Ru *3p* peaks were observed at 466.2 and 488.5 eV. This Ru(0) $3p_{3/2}$ and $3p_{1/2}$ doublet resulted from spin-orbit splitting (Fig. 3E). The O *1s* peak at 531.83 eV indicated an oxygen (O^{2-}) species on the product surface and confirmed the presence of an iron oxide species. The Binding Energy Lookup Table for Signals from Elements and Common Chemical Species list values for the species discussed above: Fe$2p_{3/2}$ = 710.7 eV, Fe$2p_{1/2}$ = 719.9 eV, Co$2p_{3/2}$ = 778.3 eV, Co$2p_{1/2}$ = 793.7 eV, Ru$3d_{5/2}$ = 280.1 eV, Ru$3d_{3/2}$ = 284.2 eV, Ru$3p_{3/2}$ = 466.1 eV, Ru$3p_{1/2}$ = 488.4 eV [37] Notably, the metallic bonding energies within the synthesised Ru-capped/FeCo nanoflowers were slightly shifted from each component's reference atomic orbital

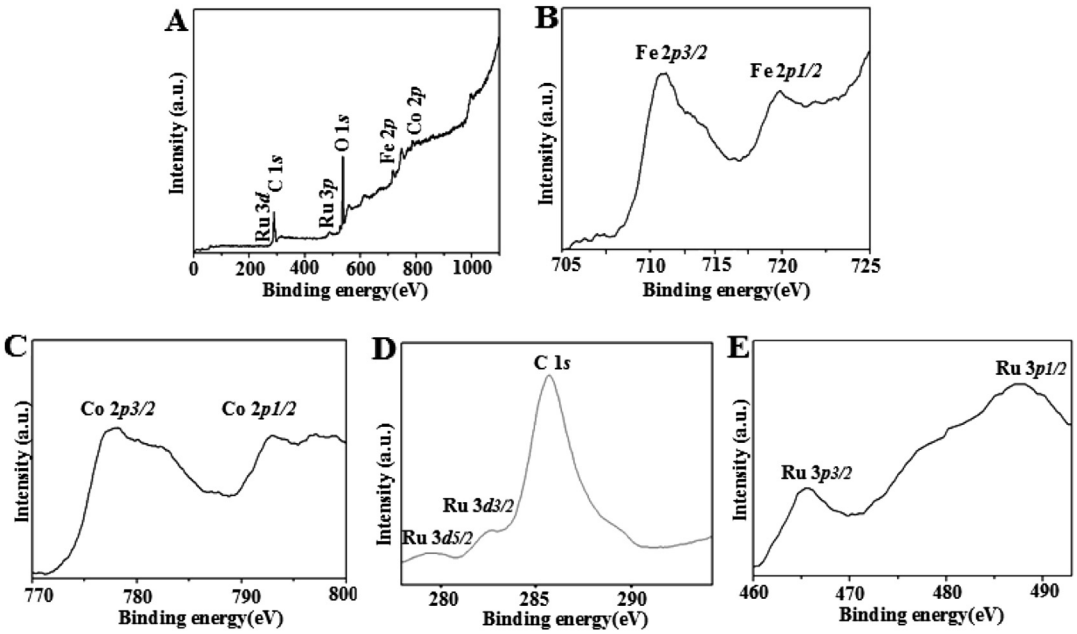

Fig. 3. XPS of Ru-capped/FeCo nanoflowers(A) with detailed spectra of Fe *2p* (B), Co *2p* (C), Ru *3d* (D) and Ru *3p* (E). All of the horizontal axes represent the binding energies corrected for C *1s*.

binding energy. These shifts are explained by the different chemical environment of Fe, Co and Ru in the synthesized Ru-capped/FeCo nanoflowers with respect to pure iron, cobalt and ruthenium metals.

3.3. Magnetic properties

Fig. 4A plots the room temperature hysteresis loops of FeCo/Ru nanostructures having different compositions. The saturation magnetisation (Ms) and coercivity (Hc) were related to the Fe and Co molar ratio. The Ms values obtained were 173.39, 155.01, 136.88, 118.81, 105.61 and 90.12 emu g^{-1} for $Fe_{65}Co_{30}/Ru_5$, $Fe_{55}Co_{40}/Ru_5$, $Fe_{45}Co_{50}/Ru_5$, $Fe_{32}Co_{63}/Ru_5$, $Fe_{22}Co_{73}/Ru_5$ and $Fe_{11}Co_{84}/Ru_5$, respectively. The corresponding Hc values were 213.31, 264.16, 309.96, 378.16, 708.14 and 534.11 Oe. In Fig. 4B, the two broken lines show Ms and Hc plotted against Fe/Co molar ratio for the FeCo/Ru nanostructures. Increases in Co content led to increases in Hc but decreases in Ms. The maximum Ms (173.39 emu g) was observed in the $Fe_{65}Co_{30}/Ru_5$ nanostructure, whereas the maximum Hc (708.14 Oe) was observed in the $Fe_{22}Co_{73}/Ru_5$ nanostructure. These observations were consistent with data for reported FeCo nanoalloys [38]. The synthesised Ru-capped/FeCo nanoflowers respond to magnets because of their inherent magnetic properties. In this case, the synthesised FeCo/Ru nanostructures, when suspended in water, quickly responded to magnets. The nanostructures were easily recovered by an external magnet and then readily redispersed in water using stirring or sonication. Hence, the synthesised materials exhibited promise for recyclable applications.

4. Dehydrogenation catalytic activity

Under ambient pressure and at room temperature, the catalytic activity of the synthesised FeCo/Ru hierarchical nanostructures towards $NaBH_4$ hydrolytic dehydrogenation was evaluated. The following equation expresses the hydrolysis of $NaBH_4$ [39].

The initial concentration of NaOH was varied from 0 M to 0.75 M to test its effect on the hydrolysis of $NaBH_4$ (0.21 M, 10 mL). The results are graphed in Fig. 5A. The dehydrogenation rate increased drastically from no NaOH (Trace (a)) and reached its maximum at a NaOH concentration of 0.375 M (Trace (c)). Further increases in NaOH concentration reduced the dehydrogenation rate, and the dehydrogenation rate at 0.75 M was lower than the dehydrogenation

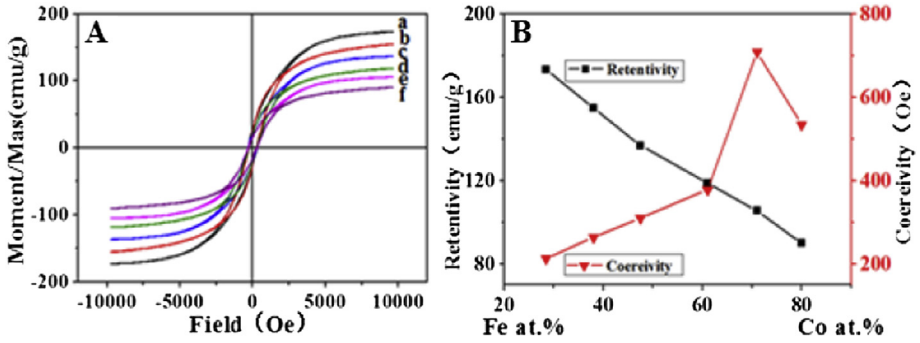

Fig. 4. (A) Room-temperature hysteresis loops of FeCo/Ru nanoalloys with differing compositions: $Fe_{65}Co_{30}/Ru_5$ (a), $Fe_{55}Co_{40}/Ru_5$ (b), $Fe_{45}Co_{50}/Ru_5$ (c), $Fe_{32}Co_{63}/Ru_5$ (d), $Fe_{22}Co_{73}/Ru_5$ (e), $Fe_{11}Co_{84}/Ru_5$ (f). (B) Variation of *Ms* and *Hc* with Co and Fe content (at.%).

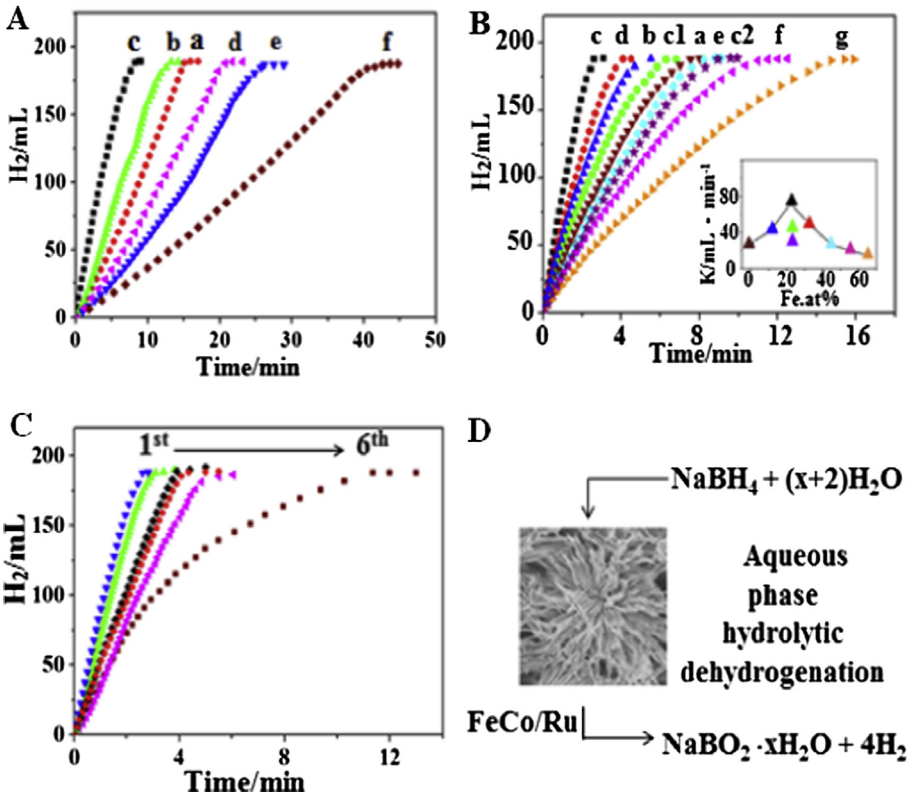

Fig. 5. (A) Aqueous $NaBH_4$ dehydrogenation catalysed by $Fe_{45}Co_{50}/Ru_5$ cap-nanoflowers using NaOH concentrations of 0 M (15.1 min) (a), 0.25 M (13.2 min) (b), 0.375 M (8.2 min) (c), 0.5 M (20.7 min) (d), 0.625 M (26.2 min) (e), 0.75 M (42.6 min) (f); (B) Aqueous $NaBH_4$ (0.21 M, 10 mL) dehydrogenation with NaOH (0.375 M, 10 mL) catalysed by FeCo/Ru nanoalloys in differing compositions: a) $Co_{95}Ru_5$; b) $Fe_{11}Co_{84}/Ru_5$; c) $Fe_{22}Co_{73}/Ru_5$, c1) $Fe_{22}Co_{73}/Ru_5$, c2) $Fe_{24}Co_{76}$; d) $Fe_{32}Co_{63}/Ru_5$; e) $Fe_{45}Co_{50}/Ru_5$; f) $Fe_{55}Co_{40}/Ru_5$; g) $Fe_{65}Co_{30}/Ru_5$; (C) Dehydrogenation catalysed by $Fe_{22}Co_{73}/Ru_5$ cap-nanoflowers under ambient pressure and r.t., from the 1st to 6th run of the lifetime experiment; (D) A schematic representation of hydrolytic dehydrogenation.

rate without NaOH. The effect of NaOH concentration on $NaBH_4$ hydrolysis greatly depends on the type of catalyst [27]. Ru-based catalytic systems are adversely affected by increasing NaOH concentration, whereas some Co-based systems are reported as showing increased activity with increased NaOH concentrations. In our case, Ru-capped/FeCo nanoflowers catalyst exhibited the best catalytic activity when the NaOH concentration was 0.375 M Fig. 5B plots the amount of H_2 generated as a function of reaction time for synthesised FeCo/Ru catalysts with different shapes and compositions. The $Fe_{22}Co_{73}/Ru_5$ cap-nanoflowers (Curve (c)) completed the dehydrogenation reaction faster than the $Fe_{22}Co_{73}/Ru_5$ nanospheres (Curve (c1)) 3.1 min and 6.1 min, respectively. Therefore, morphology affects FeCo/Ru catalytic activity towards $NaBH_4$ hydrolytic dehydrogenation. For the Fe:Co ratio of 22:73, Ru-containing Ru-capped/FeCo nanoflowers exhibited markedly higher catalytic activity than the FeCo nanorods without Ru (Curve (c2), 10 min). This observed high catalytic efficiency towards $NaBH_4$ hydrolysis is explained by the ligand effects and strain exerted by Co and Ru [28,39–41] on the width of the surface Co d-band Ru-capped/FeCo nanoflowers. The dehydrogenation rate of $NaBH_4$ greatly depends on the type of catalysts used in the reaction [42,43].

The effect of differing Fe:Co molar ratios in FeCo/Ru on $NaBH_4$ hydrolytic dehydrogenation was explored by varying the Fe content from 0% to 65%. The largest hydrogen generation rate was obtained at 22% Fe (Curve (c)). The hydrogen generation rate increased with the Fe increase from 0% to 22%. The maximum hydrogen generation rate was approximately 2.6 times of the rate of the reaction catalysed by Co_{95}/Ru_5 (Curve (a)). However, increasing Fe content further decreased the rate of hydrogen generation. Particularly, when Fe content reached or exceeded 45%, the rate was lower than the rate for Co_{95}/Ru_5 (Curve (a)). The graph of H_2 generation rate versus Fe% is illustrated in the Fig. 5B inset. A small quantity of Fe dissolved in FeCo/Ru catalysts is favourable to the distribution of Co active sites. Nevertheless, as the Fe content increased, Fe began to physically cover some Co active sites. Finally, the $Fe_{22}Co_{73}/Ru_5$ cap-nanoflowers exhibited the largest activity.

Additionally, the lifetime of the synthesised Ru-capped/FeCo nanoflowers was examined by testing the catalytic activity of $Fe_{22}Co_{73}/Ru_5$ over six sequential $NaBH_4$ hydrolysis reactions at ambient pressure and r.t. As shown in Fig. 5C, a small decrease in catalytic activity was observed over the first five reactions, with the reaction time increasing only slightly from 3.1 min to 8.3 min. The reaction time for the sixth reaction was 13 min. In the presence of a catalyst, the hydrolysis of basic, aqueous sodium borohydride solution was exothermic and afforded two fold more hydrogen than expected, when based on the equation in the Fig. 5D [39].

The hydrolytic dehydrogenation of $NaBH_4$ is temperature sensitive. Therefore, the influence of temperature on dehydrogenation rates was studied in $NaBH_4$ solution (0.21 M) containing $Fe_{22}Co_{73}/Ru_5$ catalyst at a 0.124 catalyst/$NaBH_4$ molar ratio. The H_2 generation rate increased from 4293.75 to 25000.02 mL min^{-1} g^{-1} when the temperature increased from 293 K to 323 K (Fig. 6A). At each reaction temperature, the hydrogen generated linearly increased with the reaction time, indicating a zero order reaction [44,45]. Because of this zero-order, the Arrhenius equation was used to calculate the activation energy of the $NaBH_4$ hydrolysis when the synthesised $Fe_{22}Co_{73}/Ru_5$ cap-nanoflowers was utilised as catalysts. A linear fit of the Arrhenius plot of ln(r) versus $1/T$ (Fig. 6B) revealed

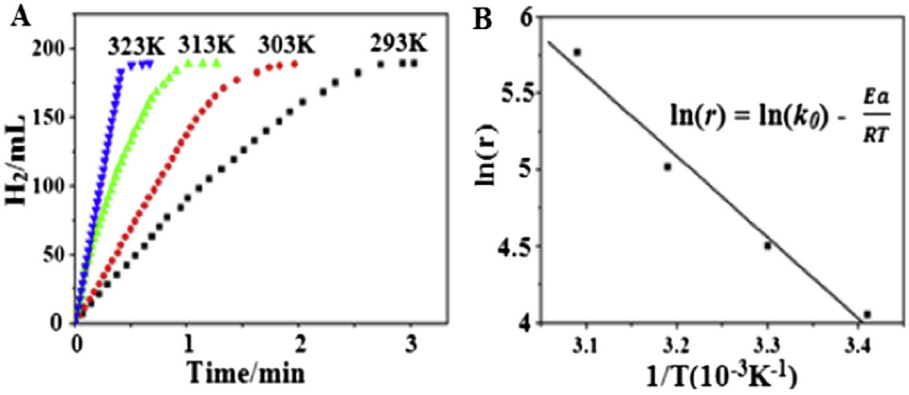

Fig. 6. (A) Dehydrogenation catalysed by $Fe_{22}Co_{73}/Ru_5$ cap-nanoflowers at reaction temperatures of 293 K, 303 K, 313 K and 323 K (from right to left); (B) Arrhenius plot for the hydrolytic dehydrogenation of $NaBH_4$ solution using $Fe_{22}Co_{73}/Ru_5$ cap-nanoflowers as catalysts. (In the inserted equation, r: the reaction rate (ml min^{-1} g^{-1}), k_0: the reaction constant (mol min^{-1} g^{-1}), Ea: the reaction activation energy (kJ mol^{-1}), *R*: the universal gas constant, *T* (K): the reaction temperature.) ($NaBH_4$ aqueous (0.21 M, 10 mL), NaOH (0.375 M, 10 mL) Catalyst/$NaBH_4$ = 0.124 (molar ratio)).

the activation energy as 42.95 kJ mol^{-1}, which is lower than the activation energy of many catalysts made of unitary transition metals—e.g., 57.62 kJ mol^{-1} for Ag—Ni core—shell NPs, 47 kJ mol^{-1} for Ru catalysts, 52.73 kJ mol^{-1} for Ni—Ru nanocomposite, and 63 kJ mol^{-1} for Raney Ni [45–49].

5. Conclusion

In conclusion, magnetic Ru-capped/FeCo nanoflowers are successfully synthesised through a solvothermal method that involved a self-catalytic growth and assembly process. Ru was observed to cap the surface of the nanoflowers. Under the optimal conditions of 0.21 M $NaBH_4$ and 0.375 M NaOH, the resultant Ru-capped/FeCo nanoflowers exhibit highly efficient catalytic activity towards the $NaBH_4$ hydrolysis at ambient pressure. Particularly, an appropriate quantity of Fe in the composition improved catalytic activity. The most catalytically efficient $Fe_{22}Co_{73}/Ru_5$ cap-nanoflowers exhibited a $NaBH_4$ dehydrogenation rate of 4293.75 ml min^{-1} g^{-1} and a low calculated activation energy (42.95 kJ mol^{-1}) compared with unitary catalysts.

Acknowledgements

This work was financially supported by the National Natural Science Foundation of China (Nos: 21171130, 51271132, 51072134 and 91222103) and 973 Project of China (No: 2011CB932404).

References

[1] D. Xu, Z. Liu, H. Yang, Q. Yang, J. Zhang, J. Fang, S. Zou, K. Sun, Angew. Chem. Int. Ed. 48 (2009) 4217.
[2] C.H. Jun, Y.J. Park, Y.R. Yeon, J.R. Choi, W.R. Lee, S.J. Ko, J. Cheon, Chem. Commun. 15 (2006) 1619.
[3] X.J. Liu, C. Zheng, L. Liang, X.D. Lei, J.F. Liu, X.M. Sun, J. Mater. Chem. 22 (2012) 7232.
[4] D. Mao, J. Yao, X. Lai, M. Yang, J. Du, D. Wang, Small 7 (2011) 578.
[5] J.T. Zhang, J.F. Liu, Q. Peng, X. Wang, Y.D. Li, Chem. Mater. 18 (2006) 867.
[6] X.L. Li, T.J. Lou, X.M. Sun, Y.D. Li, Inorg. Chem. 43 (2004) 5442.
[7] Y.C. Zhu, Q.C. Ruan, F.F. Xu, Nano Res. 2 (2009) 688.
[8] D. Chen, J. Xu, Z. Xie, G. Shen, ACS Appl. Mater. Interfaces 3 (2011) 2112.
[9] X. Chen, Z. Guo, W.H. Xu, H.B. Yao, M.Q. Li, J.H. Liu, X.J. Huang, S.H. Yu, Adv. Funct. Mater. 21 (2011) 2049.
[10] Y.Z. Sun, M. Wen, Q.S. Wu, Q. N Wu, ChemPlusChem 78 (2013) 375.
[11] H. Zeng, S.H. Sun, Adv. Funct. Mater. 18 (2008) 391.
[12] S.K. Singh, Q. Xu, Chem. Commun. 46 (2010) 6545.
[13] D.S. Wang, Y.D. Li, J. Am. Chem. Soc. 132 (2010) 6280.
[14] H.A. Esfahani, L. Wang, Y. Yamauchi, Chem. Commun. 46 (2010) 3684.
[15] D. Mott, J. Luo, P.N. Njoki, Y. Lin, L.Y. Wang, C.J. Zhong, Catal. Today 122 (2007) 378.
[16] R. Massard, D. Uzio, C. Thomazeau, C. Pichon, J.L. Roussed, J.C. Bertolini, J. Catal. 245 (2007) 133.
[17] S. Joao-Sao, S. Giorgio, J.M. Penisson, C. Chapon, S. Bourgeois, C.J. Henry, Phys. Chem. B 109 (2005) 342.
[18] I.S. Hwang, J.K. Choi, H.S. Woo, S.J. Kim, S.Y. Jung, T.Y. Seong, I.D. Kim, J.H. Lee, ACS Appl. Mater. Interfaces 3 (2011) 3140.
[19] M. Wen, F. Zhang, M.Z. Cheng, Q.S. Wu, B.L. Sun, Y.Z. Sun, ChemPhysChem 12 (2011) 3573.
[20] C.X. Xu, L. Wang, X.L. Mu, Y. Ding, Langmuir 26 (2010) 7437.
[21] M. Wen, M.Z. Cheng, S.Q. Zhou, Q.S. Wu, N. Wang, L.Y. Zhou, J. Phys. Chem. C 116 (2012) 11702.
[22] S.H. Joo, J.Y. Park, J.R. Renzas, D.R. Butcher, W. Huang, G.A. Somorjai, Nano. Lett. 10 (2010) 2709.
[23] M. Zahmakıran, M. Tristany, K. Philippot, K. Fajerwerg, S. Özkar, B. Chaudret, Chem. Commun. 46 (2010) 2938.
[24] Y.T. Kim, H. Lee, H.J. Kim, T.H. Lim, Chem. Commun. 46 (2010) 2085.
[25] S. Alayoglu, P. Zavalij, B. Eichhorn, Q. Wang, A.I. Frenkel, P. Chupas, ACS Nano. 3 (2009) 3127.
[26] Y.W. Lee, M. Kim, Z.H. Kim, S.W. Han, J. Am. Chem. Soc. 131 (2009) 17036.
[27] M. Nie, Y.C. Zou, Y.M. Huang, J.Q. Wang, Int. J. Hydrogen Energy 37 (2012) 1568.
[28] F. Tao, M.E. Grass, Y.W. Zhang, D.R. Butcher, J.R. Renzas, Z. Liu, J.Y. Chung, B.S. Mun, M. Salmeron, G.A. Somorjai, Science 322 (2008) 932.
[29] B.L. Davis, D.A. Dixon, E.B. Garner, J.C. Gordon, M.H. Matus, B. Scott, F.H. Stephens, Angew. Chem. Int. Ed. 48 (2009) 6812.
[30] B.H. Liu, Q. Li, Int. J. Hydrogen Energy 33 (2008) 7385.
[31] X.W. Zhang, J.Z. Zhao, F.Y. Cheng, J. Liang, Z.L. Tao, J. Chen, Int. J. Hydrogen Energy 35 (2010) 8363.
[32] H.X. Li, H. Li, W.L. Dai, M.H. Qiao, Appl. Catal. A: Genet. 238 (2003) 119.
[33] H.J. Zhai, J. Li, L.S. Wang, J. Chem. Phys. 121 (2004) 8369.
[34] Y.C. Zou, Y.M. Huang, X. Li, H.L. Liu, Int. J. Hydrogen Energy 36 (2011) 4315.
[35] T. Jacob, W.A. Goddard, J. Phys. Chem. B 108 (2004) 8311.
[36] V.K. LaMer, R.H. Dinegar, J. Am. Chem. Soc. 72 (1950) 4847.
[37] B.V. Crist, XPS International. Inc, 1999.
[38] G.S. Chaubey, C. Barcena, N. Poudyal, C.B. Rong, J.M. Gao, S.H. Sun, J.P. Liu, J. Am. Chem. Soc. 129 (2007) 7214.
[39] N. Sahiner, O. Ozay, E. Inger, N. Aktas, Appl. Catal. 102 (2011) 201.
[40] J.R. Kitchin, J.K. Nørskov, M.A. Barteau, J.G. Chen, Am. Phys. Soc. 93 (2004) 156801.
[41] R.J. Keaton, J.M. Blacquiere, R.T. Baker, J. Am. Chem. Soc. 129 (2007) 1844.
[42] N. Patel, R. Fernandes, A. Miotello, J. Power Sources 188 (2009) 411.
[43] M. Wen, B.L. Sun, B. Zhou, Q.S. Wu, J. Peng, J. Mater. Chem. 22 (2012) 11988.
[44] F.Y. Cheng, H. Ma, Y.M. Li, J. Chen, Inorg. Chem. 46 (2007) 788.
[45] C.H. Liu, B.H. Chen, C.L. Hsueh, J.R. Ku, M.S. Jeng, F. Tsau, Int. J. Hydrogen Energy 34 (2009) 2153.
[46] S.C. Amendola, S.L. Sharp-Goldman, M.S. Janjua, N.C. Spencer, M.T. Kelly, P.J. Petillo, M. Binder, Int. J. Hydrogen Energy 25 (2000) 969.
[47] M.C. Denney, V. Pons, T.J. Hebden, D.M. Heinekey, K.I. Goldberg, J. Am. Chem. Soc. 128 (2006) 12048.
[48] M.E. Bluhm, M.G. Bradley, R. Butterick, U. Kusari, L.G. Sneddon, J. Am. Chem. Soc. 128 (2006) 7748.
[49] B.L. Sun, M. Wen, Q.S. Wu, J. Peng, Adv. Funct. Mater. 22 (2012) 2860.